Research Article

Interconnected CeO$_2$ Nanofibers for Enhanced CO Gas Sensing

Wenchao Zhang [ID],[1] Nie Zhao,[2] Yongrong Liu,[3] and Bo Li [ID][3]

[1]*Department of Anesthesiology, Beijing Jishuitan Hospital, Beijing, China*
[2]*College of Materials Science and Engineering, Xiangtan University, Xiangtan, 411105 Hunan Province, China*
[3]*Operation Center, The Third Xiangya Hospital of Central South University, Changsha, 410013 Hunan Province, China*

Correspondence should be addressed to Bo Li; liboxysxy@qq.com

Developing a new type of CO gas sensor with high response, good reproducibility, and short response/recovery time is of great significance in medical fields, especially during anesthesia. During mechanical ventilation, CO gas will be produced by CO$_2$ absorbent. Herein, novel interconnected CeO$_2$ nanofibers with an average diameter of 150 nm are firstly prepared by electrospinning. The results show that the received nanofibers are mainly composed of fluorite-structured CeO$_2$ crystals with oxygen vacancies as well as the adsorbed oxygen species on the fiber surface. It is found that there is no agglomeration and sintering for the nanofibers even after annealing at 1000°C. The interconnected nanofibers exhibit excellent gas sensing performance to CO gas at an optimum operating temperature of 450°C, where the gas sensing response value is 2.82. And the nanofibers also exhibit excellent gas sensing reproducibility, fast response/recovery rate (2 s/4 s), and high response value-concentration correlation toward CO. This study provides a simple approach to interconnected CeO$_2$ nanofibers for potential gas sensor application.

1. Introduction

In industry, carbon monoxide (CO) is the basis of monocarbon chemistry, which is mainly used for the production of methanol and phosgene and organic synthesis, and has a very important medical application value [1–3]. However, under normal circumstances, CO is a colorless, tasteless, but highly toxic gas [4]. At a relatively high concentration, people show symptoms of poisoning to varying degrees, which harm the brain, heart, liver, kidney, lung, and other tissues of the human body, and the minimum lethal concentration for human inhalation is 5000 ppm (5 minutes) [5, 6]. According to the ordinances of the National Institute of Occupational Safety and Health, the lethiferous exposure concentration and endurance of CO gas is 35 ppm for endurance of 10 h and 50 ppm for endurance of 8 h [7]. Therefore, it is particularly important to monitor CO leakage in the synthesis and application of CO as fast as possible [8].

A semiconductor gas sensor is the most common low-cost gas sensor [9]. A metal oxide semiconductor not only has good chemical and thermal stability but also has excellent gas sensing properties, so it has become a hot research topic all over the world [10, 11]. Among many metal oxides, cerium dioxide (CeO$_2$) is one of the most promising gas sensing materials because of its abundant reserves, low cost, excellent thermal and structural stability, and abundant oxygen vacancies in its crystal structure [12–14]. It is also one of the most promising materials in the field of gas sensing [15]. For example, Wang et al. synthesized silica doped CeO$_2$ nanostructure as NH$_3$ gas sensors, which achieved a 0.5 ppm detection limit and 3244% response to 80 ppm NH$_3$ [16]. But usually, CeO$_2$ nanomaterials are easy to agglomerate, which makes the gas sensing performance of CeO$_2$ nanomaterials decrease rapidly [17]. Compared with nanoparticles, 1D nanofibers have a large aspect ratio, which means that more surface atoms are involved in the surface gas-solid reaction. 1D nanofibers are more stable and do not agglomerate to clumps at high temperatures. Additionally, they provide a simple one-way electron transport and numerous reaction centers compared to higher dimensional
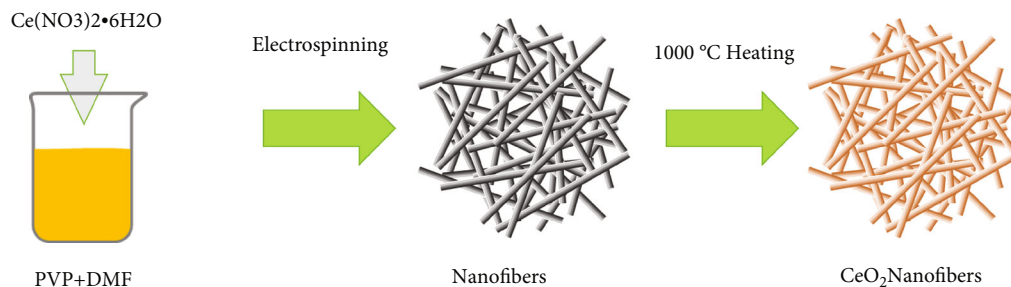
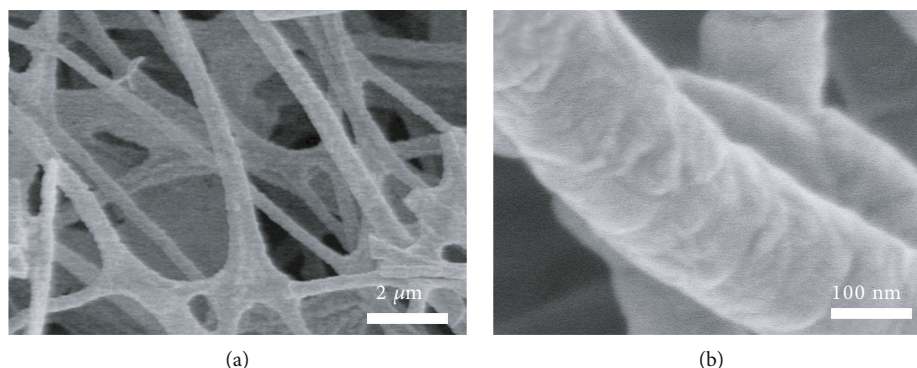SCHEME 1: Synthesis of CeO$_2$ nanofibers from electrospinning.

(a)

(b)

FIGURE 1: SEM images of the interconnected CeO$_2$ nanofibers: (a) low magnification; (b) large magnification.

nanostructures, thus maintaining a long period of fast response properties [18].

In this paper, novel interconnected CeO$_2$ nanofibers are successfully prepared by electrospinning and heat treatment. The interconnected CeO$_2$ nanofibers are connected with each other, which is beneficial to electron transfer. The results show that CeO$_2$ nanofibers have good responsiveness to CO of 10-100 ppm and good reproducibility to the same 100 ppm CO for three times, which indicates that CeO$_2$ nanofibers are a good CO gas sensing material. However, the reported optimal temperature of CeO$_2$ nanofibers is 800°C, and the response/recovery time is long. How to reduce the optimal temperature of CeO$_2$ nanofibers and improve the response/recovery rate is a great challenge.

2. Experimental and Characterization

2.1. Synthesis of CeO$_2$ Nanofibers. CeO$_2$ nanofibers were prepared by the electrospinning method (Scheme 1). In order to find the proper concentration of the spinning solution, four groups of spinning solutions with different concentrations were designed. Firstly, PVP and Ce(NO$_3$)$_2$·6H$_2$O were dissolved into the DMF to form a uniform and transparent solution, where the weight concentration of Ce(NO$_3$)$_2$·6H$_2$O was 10.50 wt%, 10.0 wt%, 9.5 wt%, and 9.0 wt%, respectively. In electrospinning, the distance between the reeling plate and the needle was controlled at 20 cm, the temperature was approximately 20°C, the humidity was approximately 40%RH, the feed rate was 1 mL/h, and the spinning voltage was 20 kV. When the spinning was stabilized, the white fiber can be seen to be ejected evenly from the needle and distrib-
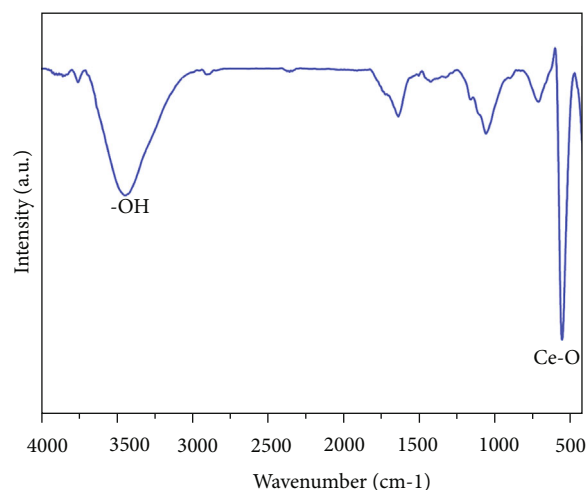

FIGURE 2: FT-IR spectrum of the interconnected CeO$_2$ nanofibers.

uted in a disc shape on the filament receiving plate. The collected fiber mat was milky white. After that, the white CeO$_2$ nanofibers can be prepared by heating the polymer fiber at 1000°C for 3 h with a ramping rate of 5°C/min.

2.2. Characterization. X-ray diffraction (XRD) is characterized on a Japanese TTRAX III X-ray diffractometer with the light source of CuKα ray, while the wavelength is 0.15418 nm. The acceleration voltage is set to 20 kV, and the scanning range is set to 10~90°. The data were analyzed using MDI Jade 6.0 software and the Scherrer formula of
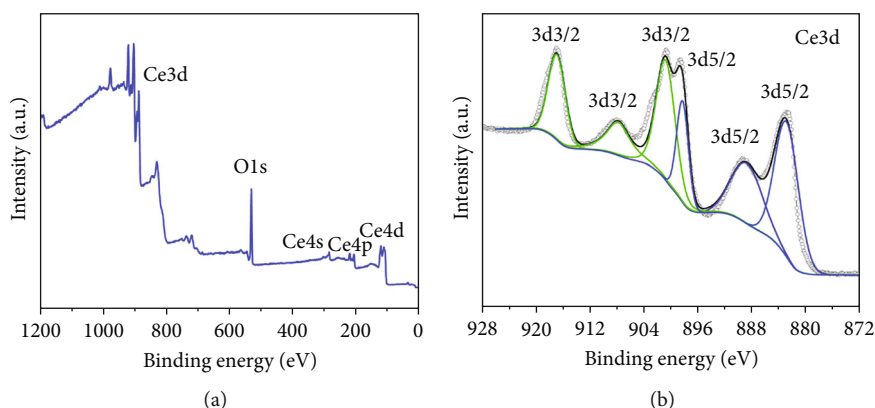
(a)

(b)

FIGURE 3: The XPS spectrum of the interconnected CeO$_2$ nanofibers: (a) survey spectrum; (b) Ce3d spectra.

$D = K\lambda/\beta COS\theta$ (D is the average size of crystal particle, K is the Scherrer coefficient (0.89), β is the peak HWHM, and θ is the diffraction angle); λ is the wavelength of X-ray (0.15406 nm) used to calculate the average size of crystal particles of gas sensing materials. A scanning electron microscope (SEM) was observed and characterized by Hitachi Field Emission SEM of Hitachi Model S-4800.

Fourier-transform infrared (FT-IR) spectra of samples in KBr pellets were obtained with a PerkinElmer spectrometer at the measuring range of 400-4000 cm^{-1}. X-ray photoelectron spectroscopy (XPS) was recorded on a Thermo Scientific ESCALAB 250Xi machine with Al Ka as the excitation source.

2.3. Gas Sensing Tests. Gas sensing tests were performed on a commercial CGS-8 Gas Sensing Measurement System. The gas sensor was fabricated by pasting a viscous slurry of the obtained sample onto an alumina tube which was positioned with a pair of Au electrodes and four Pt wires on both ends of the tube. The test substrate was prepared by mixing 0.1 g nanofiber sample with 0.1 mL terpineol to form a homogeneous paste, and then, the paste was carefully coated on the side heating alumina ceramic tube electrode. The outer diameter of the alumina ceramic tube was 1.2 mm, and the length was 4 mm. A Ni-Cr heating wire (diameter = 0.5 mm, resistance = 35 Ω) was inserted into the tube to form an indirect-heated gas sensor. Ra/Rg was usually used to characterize the response value of the gas sensing material when the resistance decreases after contacting the detection gas. Among them, Ra and Rg were the resistance of the sensor in air and after contact with the gas. Response time (t_{res}) and recovery time (t_{rec}) were defined as the time required to achieve a 90% change in sensor resistance, respectively.

3. Results and Discussion

A SEM photograph of the interconnected CeO$_2$ nanofiber samples is shown in Figure 1. It can be found that the nanofiber can keep good morphology after annealing at 1000°C for 3 hours in air atmosphere, and the nanofiber has a high aspect ratio. The average diameter of the received CeO$_2$ nanofibers was 150 nm, and the diameter was uniform. From the surface morphology of nanofibers, it can be seen that the
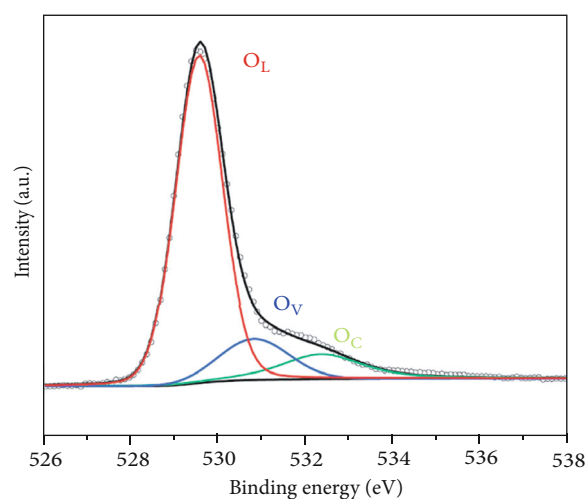

FIGURE 4: The O1s splitting pattern of CeO$_2$ nanofibers.

fibers are composed of many nanoparticles with a relatively small particle size between 20 and 40 nm. This may have resulted from the long annealing time for 3 h at 1000°C, so that the CeO$_2$ crystal size of nanofibers grows up. However, such large grains in the nanofibers can also effectively reduce the carrier loss due to the fewer grain boundaries.

The interconnected CeO$_2$ nanofibers were analyzed by FT-IR, and the results are shown in Figure 2. The absorption peak near 3400 cm^{-1} in the FT-IR spectrum is the absorption peak of -OH in air, while the peak near 547 cm^{-1} is the characteristic absorption peak of Ce-O stretch vibration [19]. This has supported the presence of CeO$_2$, which consisted in the nanofibers.

The composition and surface states of CeO$_2$ nanofibers were further characterized by XPS. Figure 3(a) is the full XPS spectrum of interconnected nanofibers. It can be seen that there are obvious spectrum lines of Ce3d, Ce4s, Ce4p, Ce4d, and O1s in the sample, indicating that there are only Ce and O elements in the fiber and no other impurities. The presence of the Ce element is analyzed by peaking the Ce3d spectra, as shown in Figure 3(b). The characteristic peaks of 916.7, 907.6, 900.8, 898.4, 888.9, and 882.7 eV obtained by dividing the peak of Ce3d spectra are all typical
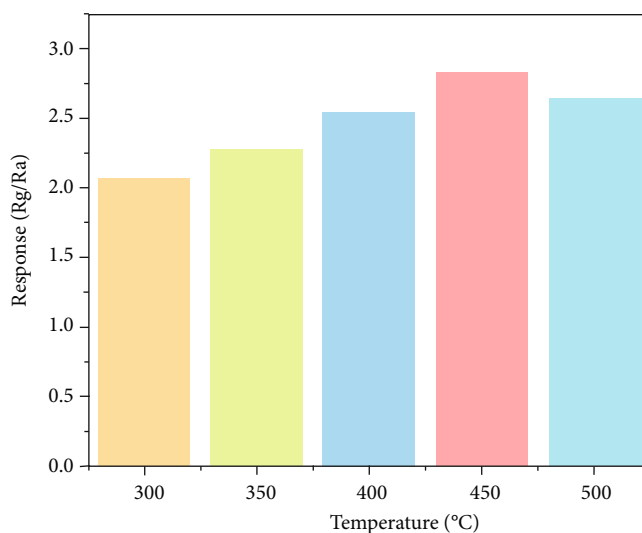
FIGURE 5: The effect of working temperature on the gas sensing response of CeO_2 nanofibers.
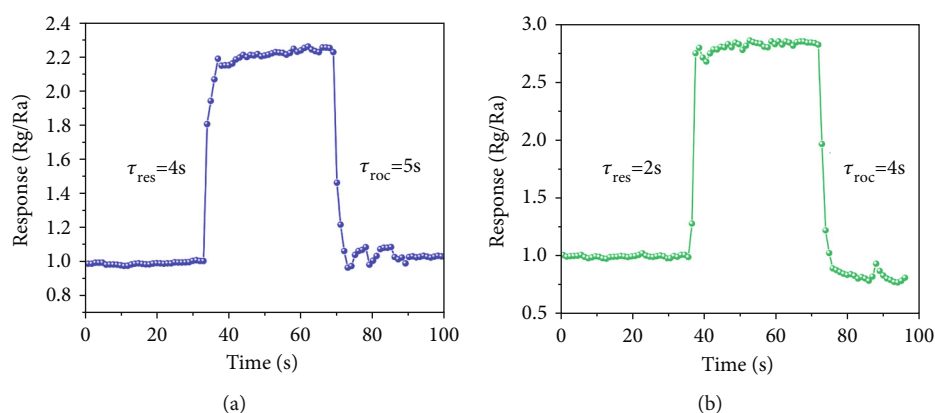

(a)

(b)

FIGURE 6: The response/recovery time of interconnected CeO_2 nanofibers to 500 ppm CO gas: (a) 350°C and (b) 450°C.

peaks of the Ce (IV) oxidation state [20]. Among them, the peaks at the binding energy of 916.7, 907.6, and 900.8 eV are the characteristic peaks of Ce element 3d3/2 orbitals, and the peaks at 898.4, 888.9, and 882.7 eV are characteristic peaks of Ce element 3d5/2 orbitals, indicating the Ce (III) oxidation state synthesized with Ce (IV) oxidation state in the samples. This demonstrates that oxygen vacancies existed in the CeO_2 nanofibers [19, 21].

Figure 4 is an O1s splitting pattern of CeO_2 nanofibers. For O1s, three main peaks at the binding energy of 532.3, 530.9, and 529.6 eV were obtained. The O_L peak at 529.6 eV was the diffraction peak of lattice oxygen in the CeO_2 phase, while the O_C peak at 532.3 eV was mainly chemically adsorbed oxygen species (O_2^-, O^{2-}, and O^-) [22]. The O_V peaks at 530.9 eV were corresponding to oxygen vacancies in the CeO_2 crystals, which were likely to cause the encouraging gas sensing by the oxygen vacancy defects [21, 23]. Therefore, according to XPS analysis, the pure CeO_2 nanofibers were composed of CeO_2 crystals, oxygen vacancies, and adsorbed oxygen species.

The effect of working temperature on the gas sensing performance of interconnected CeO_2 nanofibers toward 500 ppm CO was investigated. The results are shown in Figure 5. It was found that the response of CeO_2 nanofibers to CO gas increases first and then decreases with the increase of working temperature. The optimum working temperature was 450°C, and the maximum response value of the sensor was 2.82. This is because the sensing material was in low activity at the low working temperature [24]. At the higher temperature, the gas sensing material was more active. However, when the temperature was too high (500°C), the thermal motion of the gas is intense; thus, the gas desorption tendency was stronger. Therefore, only when the gas adsorption and desorption reach the dynamic equilibrium, the response can achieve the highest, and the dynamic equilibrium temperature (approximately 450°C) was the best working temperature for CO gas sensing.

The response/recovery time is an important index to measure the gas sensing performance. The response/recovery times of interconnected CeO_2 nanofibers toward
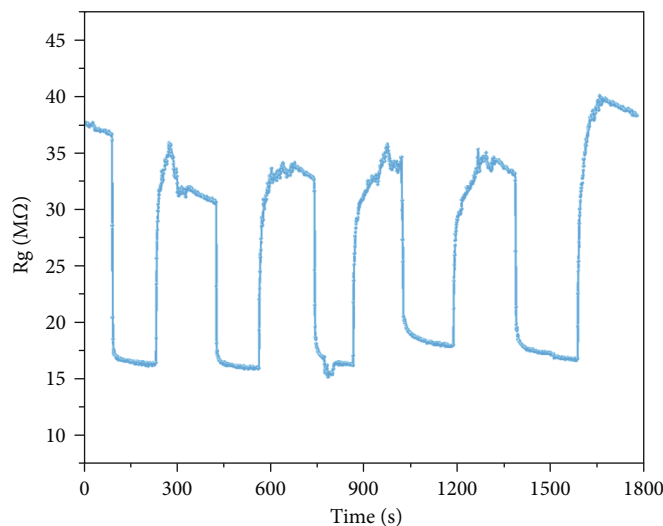
FIGURE 7: The gas sensing cycling reproducibility of interconnected CeO_2 nanofibers.
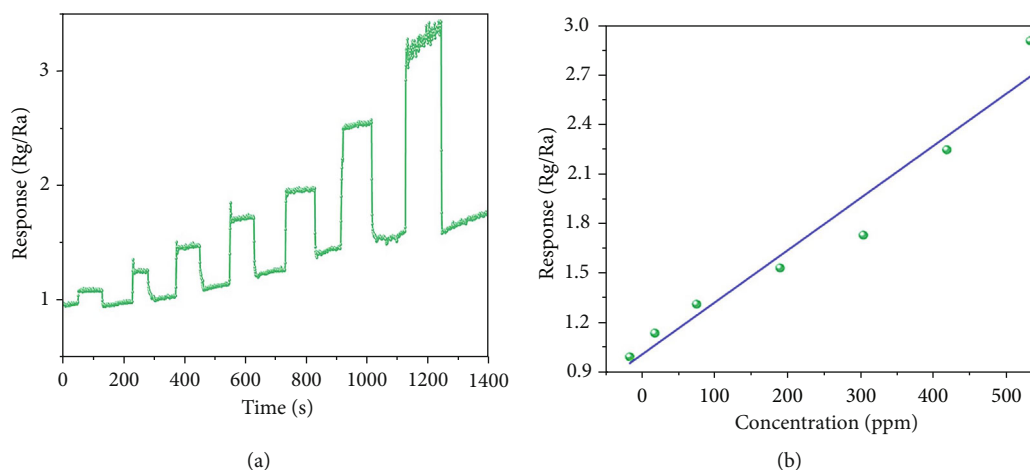

(a)

(b)

FIGURE 8: (a) The gas sensing response values of interconnected CeO_2 nanofibers toward various CO concentrations and (b) the linear fitting of sensing responses to gas concentrations.

TABLE 1: Comparison of recent reported CO sensing performance based on metal oxide gas sensors.

Materials	CO concentration (ppm)	Response	Response time (s)	Recovery time (s)	Ref.
ZnO nanoparticles	80	0.78	78	21	25
Au/CeO_2 nanoparticles	30	0.43	9	7	26
TiO_2 nanofibers	15	2.6	86	109	27
Co_3O_4 nanofibers	5	2.40	14	36	28
CuO/TiO_2 nanoparticles	50	1.77	265	554	29
CeO_2 nanofibers	500	2.82	2	4	This work

500 ppm CO gas at 350°C and 450°C are shown in Figure 6. Define the response time (t_{res}) and recovery time (t_{rec}) as 90% of the resistance value of the gas sensing material at the time of injection and release of the gas. t_{res}/t_{rec} of CeO_2 nanofibers at 350°C and 450°C are 4 s/5 s and 2 s/4 s, respectively. That is, t_{res}/t_{rec} decreases with the increasing working temperature from 350°C to 450°C. This may be ascribed to the relatively higher working temperature which can facili-

tate the thermal diffusion of the gas and increase the activity of gas sensing materials.

Sensing reproducibility reflects the stability of sensing materials to gas. Thus, it is an important index of gas sensing performance. As shown in Figure 7, the interconnected CeO_2 nanofibers were tested for gas sensing cycling reproducibility on 500 ppm CO at the optimum operating temperature 450°C. The results revealed that the response

value of CeO_2 nanofibers remained unchanged after 5 cycles, which indicated that the interconnected CeO_2 nanofibers had good gas sensing reproducibility.

Furthermore, the strong linear relationship between the sensing response and the gas concentration is very important for the gas sensors to recognize the gas concentration. Figure 8(a) shows the gas sensing response values of interconnected CeO_2 nanofibers to 20, 50, 100, 200, 300, 400, and 500 ppm CO, respectively. It can be seen that the response of the sensor increases gradually with the increasing CO concentration. The sensing response-gas concentration curve is shown in Figure 8(b), where the sensing response was fitted linearly. The correlation coefficient between the sensing responses of CeO_2 nanofibers to CO concentration was 0.954, which demonstrated that the sensing response was linearly correlated with the gas concentration.

We also compared our sensing performance with previous works on the CO sensor. As shown in Table 1, the CeO_2 nanofibers exhibit a relatively high response to CO. Particularly, the sensors based on CeO_2 nanofibers show an ultrafast response/recovery time, which is better than most of the reported CO sensors [25–29]. According to the great reproducibility, quick response/recovery, and ideally linear fitting ability, the synthesized CeO_2 nanofibers in this study showed excellent potential application in CO gas sensing.

4. Conclusions

In this paper, novel interconnected CeO_2 nanofibers were simply fabricated via the electrospinning method. The average diameter of interconnected CeO_2 nanofibers was only 150 nm, and the nanofibers were mainly composed of fluorite CeO_2 crystals, oxygen vacancies, and adsorbed oxygen species in the fibers. The received interconnected CeO_2 nanofibers showed an excellent gas sensing performance toward CO. The response of CO was first increasing and followed by decreasing as the increasing of working temperature, due to the dynamic equilibrium of gas adsorption and desorption. The optimum working temperature of the nanofibers was approximately 450°C, and the sensing response value could reach 2.82. Furthermore, the nanofiber samples revealed quick response/recovery ability, and the best response time 2 s and recovery time 4 s were tested at 450°C. The interconnected CeO_2 nanofibers also exhibit good gas sensing reproducibility among 5 cycles. In addition, the CeO_2 nanofiber exhibited a linear response-gas concentration relationship toward CO from 20 ppm to 500 ppm. This demonstrated that the CeO_2 nanofibers in this research could be a great candidate for CO sensors. And CeO_2 nanofibers may sensor the CO in the mechanical ventilation.

Data Availability

The original contributions presented in the study are included in the article/supplementary materials; further inquiries can be directed to the corresponding author.

Conflicts of Interest

The authors declare no conflict of interest.

Authors' Contributions

Conceptualization was performed by Zhao Nie and Zhang Wenchao; methodology was performed by Zhao Nie; validation was performed by Zhao Nie; formal analysis was performed by Zhang Wenchao; investigation was performed by Liu Yongrong; resources were secured by Zhao Nie; data curation was performed by Zhao Nie; writing (original draft preparation) was performed by Zhao Nie and Li Bo; writing (review and editing) was performed by Zhao Nie; visualization was performed by Zhao Nie; supervision was performed by Zhao Nie and Li Bo; project administration was performed by Li Bo; funding acquisition was performed by Li Bo. All authors have read and agreed to the published version of the manuscript.

Acknowledgments

References

[1] H. Bao, Y. Qiu, X. Peng et al., "Isolated copper single sites for high-performance electroreduction of carbon monoxide to multicarbon products," *Nature Communications*, vol. 12, no. 1, p. 238, 2021.

[2] L. McIntosh, P. Jackson, N. Hardcastle et al., "Automated assessment of functional lung imaging with 68Ga-ventilation/perfusion PET/CT using iterative histogram analysis," *European Journal of Nuclear Medicine and Molecular Imaging Physics*, vol. 8, no. 1, p. 23, 2021.

[3] G. Fan, X. Wang, X. Tu, H. Xu, Q. Wang, and X. Chu, "Density functional theory study of Cu-doped BNNT as highly sensitive and selective gas sensor for carbon monoxide," *Nanotechnology*, vol. 32, no. 7, article 075502, 2020.

[4] X. Wu, J. Lang, Z. Sun, F. Jin, and Y. H. Hu, "Photocatalytic conversion of carbon monoxide: from pollutant removal to fuel production," *Applied Catalysis B: Environmental*, vol. 295, article 120312, 2021.

[5] Q. Mao, A. T. Kawaguchi, S. Mizobata, R. Motterlini, R. Foresti, and H. Kitagishi, "Sensitive quantification of carbon monoxide in vivo reveals a protective role of circulating hemoglobin in CO intoxication," *Communications Biology*, vol. 4, no. 1, 2021.

[6] H. Cruz-Martínez, H. Rojas-Chávez, F. Montejo-Alvaro, Y. A. Peña-Castañeda, P. T. Matadamas-Ortiz, and D. I. Medina, "Recent developments in graphene-based toxic gas sensors: a theoretical overview," *Sensors*, vol. 21, no. 6, p. 1992, 2021.

[7] B. L. Risavi, R. J. Wadas, C. Thomas, and D. F. Kupas, "A novel method for continuous environmental surveillance for carbon monoxide exposure to protect emergency medical service providers and patients," *The Journal of Emergency Medicine*, vol. 44, no. 3, pp. 637–640, 2013.

[8] Q. Ouyang, L. Tu, Y. Zhang et al., "Construction of a smart nanofluidic sensor through a redox reaction strategy for

high-performance carbon monoxide sensing," *Analytical Chemistry*, vol. 92, no. 22, pp. 14947–14952, 2020.

[9] E. Fazio, S. Spadaro, C. Corsaro et al., "Metal-oxide based nanomaterials: synthesis, characterization and their applications in electrical and electrochemical sensors," *Sensors*, vol. 21, no. 7, p. 2494, 2021.

[10] S. S. Mehta, D. Y. Nadargi, M. S. Tamboli et al., "RGO/WO$_3$ hierarchical architectures for improved H$_2$S sensing and highly efficient solar-driving photo- degradation of RhB dye," *Scientific Reports*, vol. 11, no. 1, 2021.

[11] J.-H. Kim, A. Mirzaei, J. H. Bang, H. W. Kim, and S. S. Kim, "Achievement of self-heated sensing of hazardous gases by WS$_2$ (core)-SnO$_2$ (shell) nanosheets," *Journal of Hazardous Materials*, vol. 412, pp. 125–196, 2021.

[12] Q. Meng, J. Cui, Y. Tang et al., "Solvothermal synthesis of dual-porous CeO$_2$-ZnO composite and its enhanced acetone sensing performance," *Ceramics International*, vol. 45, no. 3, pp. 4103–4107, 2019.

[13] S. Parwaiz, M. M. Khan, and D. Pradhan, "CeO$_2$-based nanocomposites: an advanced alternative to TiO$_2$ and ZnO in sunscreens," *Materials Express*, vol. 9, no. 3, pp. 185–202, 2019.

[14] A. Yang, W. Li, J. Chu et al., "Enhanced sensing of sulfur hexafluoride decomposition components based on noble-metal-functionalized cerium oxide," *Materials and Design*, vol. 187, article 108391, 2020.

[15] Y. Liu, Y. Ding, L. Zhang, P.-X. Gao, and Y. Lei, "CeO$_2$ nanofibers for in situ O$_2$ and CO sensing in harsh environments," *RSC Advances*, vol. 2, no. 12, pp. 5193–5198, 2012.

[16] J. Wang, Z. Li, S. Zhang et al., "Enhanced NH$_3$ gas-sensing performance of silica modified CeO$_2$ nanostructure based sensors," *Sensors and Actuators B: Chemical*, vol. 255, pp. 862–870, 2018.

[17] E. Özkan, F. Badaczewski, P. Cop et al., "Peering into the formation of cerium oxide colloidal particles in solution by in situ small-angle X-ray scattering," *Langmuir*, vol. 36, no. 31, pp. 9175–9190, 2020.

[18] J. M. Xu and J. P. Cheng, "The advances of Co$_3$O$_4$ as gas sensing materials: a review," *Journal of Alloys and Compounds*, vol. 686, pp. 753–768, 2016.

[19] S. Arunpandiyan, S. Vinoth, A. Pandikumar, A. Raja, and A. Arivarasan, "Decoration of CeO$_2$ nanoparticles on hierarchically porous MnO$_2$ nanorods and enhancement of supercapacitor performance by redox additive electrolyte," *Journal of Alloys and Compounds*, vol. 861, article 158456, 2021.

[20] M. Kourtelesis, T. S. Moraes, L. V. Mattos, D. K. Niakolas, F. B. Noronha, and X. Verykios, "The effects of support morphology on the performance of Pt/CeO$_2$ catalysts for the low temperature steam reforming of ethanol," *Applied Catalysis B: Environmental*, vol. 284, article 119757, 2021.

[21] Q. Wang, Y. Chen, X. Liu, L. Li, L. Du, and G. Tian, "Sulfur doped In$_2$O$_3$-CeO$_2$ hollow hexagonal prisms with carbon coating for efficient photocatalytic CO$_2$ reduction," *Chemical Engineering Journal*, vol. 421, article 129968, 2021.

[22] C. Anandan and P. Bera, "XPS studies on the interaction of CeO$_2$ with silicon in magnetron sputtered CeO$_2$ thin films on Si and Si$_3$N$_4$ substrates," *Applied Surface Science*, vol. 283, pp. 297–303, 2013.

[23] D. Majumder and S. Roy, "Development of low-ppm CO sensors using pristine CeO$_2$ nanospheres with high surface area," *ACS Omega*, vol. 3, no. 4, pp. 4433–4440, 2018.

[24] C. R. Michel and A. H. Martínez-Preciado, "CO sensing properties of novel nanostructured La$_2$O$_3$ microspheres," *Sensors and Actuators B: Chemical*, vol. 208, pp. 355–362, 2015.

[25] M. Hjiri, F. Bahanan, M. S. Aida, L. El Mir, and G. Neri, "High performance CO gas sensor based on ZnO nanoparticles," *Journal of Inorganic and Organometallic Polymer and Materials*, vol. 30, no. 10, pp. 4063–4071, 2020.

[26] D. Majumder, A. Datta, M. K. Mitra, and S. Roy, "Kinetic analysis of low concentration CO detection by Au-loaded cerium oxide sensors," *RSC Advances*, vol. 95, pp. 92898–92995, 2016.

[27] J.-A. Park, J. Moon, S.-J. Lee, S. H. Kim, T. Zyung, and H. Y. Chu, "Structure and CO gas sensing properties of electrospun TiO$_2$ nanofibers," *Materials Letters*, vol. 64, no. 3, pp. 255–257, 2010.

[28] C. Busacca, A. Donato, M. L. Faro, A. Malara, G. Neri, and S. Trocino, "CO gas sensing performance of electrospun Co$_3$O$_4$ nanostructures at low operating temperature," *Sensors and Actuators B: Chemical*, vol. 303, article 127193, 2020.

[29] U. T. Nakate, P. Patil, S.-I. Na, Y. T. Yu, E.-K. Suh, and Y.-B. Hahn, "Fabrication and enhanced carbon monoxide gas sensing performance of p-CuO/n-TiO$_2$ heterojunction device," *Collods and Surfaces A: Physicochemical and Engineering Aspects*, vol. 612, article 125962, 2021.